Butyrate supplementation regulates expression of chromosome segregation 1-like protein to reverse the genetic distortion caused by p53 mutations in colorectal cancer

CHUN-CHAO CHANG[1,2], WEI-YU KAO[1,2], CHIH-YI LIU[3,4], HUI-HSIEN SU[1,2], YU-AN KAN[1,2], PAO-YING LIN[1,2], WEI-CHI KU[4], KANG-WEI CHANG[5,6], RUEY-NENG YANG[4,7] and CHI-JUNG HUANG[8,9]

[1]Division of Gastroenterology and Hepatology, Department of Internal Medicine, Taipei Medical University Hospital; [2]Division of Gastroenterology and Hepatology, Department of Internal Medicine, School of Medicine, College of Medicine, Taipei Medical University, Taipei 11031; [3]Department of Pathology, Sijhih Cathay General Hospital, New Taipei 22174; [4]School of Medicine, College of Medicine, Fu Jen Catholic University, New Taipei 24205; [5]Neuroscience Research Center and [6]Laboratory Animal Center, Taipei Medical University, Taipei 11031; [7]Department of Internal Medicine, Sijhih Cathay General Hospital, New Taipei 22174; [8]Department of Medical Research, Cathay General Hospital, Taipei 10630; [9]Department of Biochemistry, National Defense Medical Center, Taipei 11490, Taiwan, R.O.C.

Received December 20, 2021; Accepted March 4, 2022

DOI: 10.3892/ijo.2022.5354

Abstract. The chromosome segregation 1-like (CSE1L) protein, which regulates cellular mitosis and apoptosis, was previously found to be overexpressed in colorectal cancer (CRC) cells harboring mutations. Therefore, regulating CSE1L expression may confer chemotherapeutic effects against CRC. The gut microflora can regulate gene expression in colonic cells. In particular, metabolites produced by the gut microflora, including the short-chain fatty acid butyrate, have been shown to reduce CRC risk. Butyrates may exert antioncogenic potential in CRC cells by modulating p53 expression. The present study evaluated the association between CSE1L expression and butyrate treatment from two non-transformed colon cell lines (CCD-18Co and FHC) and six CRC cell lines (LS 174T, HCT116 $p53^{+/+}$, HCT116 $p53^{-/-}$, Caco-2, SW480 and SW620). Lentiviral knockdown of CSE1L and p53, reverse transcription-quantitative PCR (CSE1L, c-Myc and p53), western blotting [CSE1L, p53, cyclin (CCN) A2, CCNB2 and CCND1], wound healing assay (cell migration), flow cytometry (cell cycle analysis) and immunofluorescence staining (CSE1L and tubulin) were adopted to verify the effects of butyrate on CSE1L-expressing CRC cells. The butyrate-producing gut bacteria *Butyricicoccus pullicaecorum* was administered to mice with 1,2-dimethylhydrazine-induced colon tumors before the measurement of CSE1L expression. The effects of *B. pullicaecorum* on CSE1L expression were then assessed by immunohistochemical staining for CSE1L and p53 in tissues from CRC-bearing mice. Non-cancerous colon cells with the R273H p53 mutation or CRC cells haboring p53 mutations were found to exhibit significantly higher CSE1L expression levels. CSE1L knockdown in HCT116 $p53^{-/-}$ cells resulted in G_1-and G_2/M-phase cell cycle arrest. Furthermore, in HCT116 $p53^{-/-}$ cells, CSE1L expression was already high at interphase, increased at prophase, peaked during metaphase before declining at cytokinesis but remained relatively high compared with that in HCT116 expressing wild-type p53. Significantly decreased expression levels of CSE1L were also observed in HCT116 $p53^{-/-}$ cells that were treated with butyrate for 24 h. In addition, the migration of HCT116 $p53^{-/-}$ cells was significantly decreased after CSE1L knockdown or butyrate treatment. Tumors with more intense nuclear p53 staining and weaker CSE1L staining were found in mice bearing DMH/DSS-induced CRC that were administered with *B. pullicaecorum*. Taken together, the results indicated that butyrate can impair CSE1L-induced tumorigenic potential. In conclusion, butyrate-producing microbes, such as *B. pullicaecorum*, may reverse the genetic distortion caused by p53 mutations in CRC by regulating CSE1L expression levels.

Correspondence to: Dr Ruey-Neng Yang, Department of Internal Medicine, Sijhih Cathay General Hospital, 2 Lane 59 Jiancheng Road, New Taipei 22174, Taiwan, R.O.C.
E-mail: hepatoma1260@yahoo.com.tw

Dr Chi-Jung Huang, Department of Medical Research, Cathay General Hospital, 280, Section 4, Renai Road, Taipei 10630, Taiwan, R.O.C.
E-mail: aaronhuang@cgh.org.tw

Key words: colorectal cancer, chromosome segregation 1-like, *butyricicoccus pullicaecorum*, short-chain fatty acid, p53 tumor suppressor

Introduction

The overexpression of chromosome segregation 1-like (CSE1L), also known as cellular apoptosis susceptibility protein, has been previously reported to correlate positively with the

progression of various malignacies, such as gastric cancer and colorectal cancer (CRC) (1-5). However, this CSE1L-induced risk of CRC tumorigenisis can be suppressed by the activation of wild-type p53 expression (6). It has been also reported that different chemotherapeutic agents, including 5-fluorouracil, cisplatin, and paclitaxel, can mediate differential apoptotic effects in CSE1L-overexpressing CRC cancer cells (7,8). The therapeutic efficacy of drugs against CRC can be reduced through the suppression of paclitaxel-induced apoptosis in CSE1L-expressing CRC cells (8,9). Therefore, CSE1L knockdown may improve CRC treatment (8).

Gut microbes can regulate the gene expression profile in colonic cells, which may in turn alter the course of CRC (10,11). Short-chain fatty acids (SCFAs) derived from microbial metabolism in the gut, including acetate, propionate and butyrate, are key for the maintenance of intestinal homeostasis (12,13). SCFAs can induce cell apoptosis and cell cycle arrest to reduce cancer risk (14), rendering them to be potential chemotherapeutic agents (15). Butyrate-producing microorganisms in the gut have been reported to prevent necrotic enteritis and reduce pathogen abundance (16-18). Therefore, dysbiosis caused by the overpopulation of detrimental microbes and underpopulation of beneficial butyrate-producing microbes in the gut may confer clinical significance in CRC. However, the effects of butyrate in CRC and the molecular mechanism underlying such effects remain unclear (19). Butyrate has been previously documented to downregulate the expression of a number of genes, including placenta specific 8 protein, toll-like receptor 4 and glucose 6-phosphatase (10,20-22). It can attenuate the lipopolysaccharide-induced inflammation of intestinal epithelial cells whilst exerting antioncogenic potential in LS1034 or WiDr human CRC cells by promoting p53 gene expression (23-25). In particular, patients with inflammatory bowel disease or CRC were found to have lower concentrations of the butyrate-producing microbe *butyricicoccus pullicaecorum* in their stools (10,26). In addition, the culture supernatant of *B. pullicaecorum* is rich in butyrates and can strengthen intestinal barrier function (17,26), which supports the pharmabiotic potential *B. pullicaecorum* for clinical application (10,20,27,28). However, the possible association between CSE1L and/or the butyrate-producing *B. pullicaecorum* in the development of CRC remain poorly understood.

A previous study has indicated that suppression of CSE1L expression in CRC cells may improve CRC treatment (8). Butyrate-producing microorganisms in the gut have been reported to confer potentially anti-CRC effects (17). Accordingly, a possible strategy to alter CRC physiology would be to decrease CSE1L expression in CRC cells by either *B. pullicaecorum* administration or butyrate supplementation. However, information concerning the potential effects remain unavailable. Therefore, the aim of the present study was to explore the potential role of butyrate in the molecular events mediated by CSE1L in CRC cell lines with different p53 genotypes. Knockdown of CSE1L in HCT116 $p53^{-/-}$ cells, knockdown of p53 in HCT116 $p53^{+/+}$ and CRC cell lines with very distinct differences in the p53 status were applied to evaluate the effects of CSE1L on the expression levels of wild-type p53. To examine the molecular significance of butyrate supplementation on CSE1L expression and CRC alleviation, cellular physiology of buyrate-treated HCT116 $p53^{-/-}$ cells *in vitro* and the colon tumors from mice after *B. pullicaecorum* administration *in vivo* were used. In this manner, the potential role of *B. pullicaecorum* and CSE1L in CRC were investigated and clarified.

Materials and methods

Induction of CRC in mice. A total of 17 male BALB/cByJNarl mice aged 4-6 weeks, weighing 22.7±0.6 g, were provided by the National Laboratory Animal Center (National Applied Research Laboratories, Taipei, Taiwan). All animal experiments were conducted in compliance with ARRIVE (Animal Research: Reporting of In Vivo Experiments) guidelines (29). The protocols followed the principles of Reduction, Refinement and Replacement and were approved by the Institutional Animal Care and Use Committees of Cathay General Hospital (approval no. 107-008; Taipei, Taiwan). Mice (at n=3-5 per plastic cage) were housed in an individually ventilated cage rack system (Tecniplast Group) and had free access to food and drinking water under the following conditions: 50±10% humidity, 12-h light/dark cycle and 23±2˚C temperature. All efforts were made to minimize the number of mice and their suffering. The mice were classified into the following groups as previously described (17): i) Control group (n=5), consisting of mice that did not receive any chemical or *B. pullicaecorum* administration; ii) 1,2-dimethylhydrazine (DMH; cat. no. D0741; Tokyo Chemical Industry Co., Ltd.)/dextran sulphate sodium (DSS; cat. no. D5144; Tokyo Chemical Industry Co., Ltd.) group (n=6), consisting of mice that received DMH (20 mg/kg) once at the beginning of the experiment through intraperitoneal injection, followed by 1 week of normal water and 1 week of DSS (30 g/l) in the drinking water, with two cycles of additional DSS treatment (2 weeks of normal water + 1 week of DSS (30 g/l) in drinking water); and iii) DMH/DSS/B. pullicaecorum group (n=6), consisting of mice that received DMH/DSS in the same manner as DMH/DSS group, but were treated with *B. pullicaecorum* every 7 days during the experiment. The body weight of each mouse was monitored once a week. All mice were euthanized with CO_2 in a cage when they showed weakness and rapid weight loss of 15-20% or at the end of the experiment. The duration of this animal experiment was 2-3 months. The CO_2 flow rate was set to displace 30% of the cage volume per minute. Immobility for >2 min and lack of spontaneous breathing were used to confirm animal death before the colon samples were collected.

B. pullicaecorum administration by oral gavage. The molecular effects of *B. pullicaecorum* on colon tumor formation was evaluated. *B. pullicaecorum* ($3.125x10^7$ colony-forming units in 100 μl of modified peptone yeast extract broth) was administered by oral gavage. *B. pullicaecorum* (cat. no. BCRC-81109; https://catalog.bcrc.firdi.org.tw/BcrcContent?bid=81109) and the growth medium (modified peptone yeast extract broth; cat. no. 967; Bioresource Collection and Research Center) were purchased from the Bioresource Collection and Research Center (Hsinchu, Taiwan) and cultured for 3 days under anaerobic conditions (10% CO_2 and 90% N_2) at 37˚C as described previously (17).

Cell lines and reagents. In total, two human colon cell lines, CCD-18Co [cat. no. CRL-1459; American Type Culture Collection (ATCC)], which harbors wild-type p53 and FHC (cat. no. CRL-1831; ATCC), which expresses the R273H p53 mutant (30), were acquired as non-transformed colon cells (30,31). In addition, three human CRC cell lines (LS 174T, cat. no. CL-188; T84, cat. no. CCL-248; HCT116 $p53^{+/+}$, cat. no. CCL-247; all from ATCC) expressing wild-type p53, two human CRC cell lines (SW480, cat. no. CCL-228; SW620, cat. no. CCL-227; both from ATCC) carrying the R273H and P309S double p53 mutation (32), in addition to two p53-null cell lines [Caco-2, cat. no. HTB-37, ATCC; HCT116 $p53^{-/-}$, a gift from Professor Bert Vogelstein (School of Medicine, Johns Hopkins University, Baltimore, USA)] (33,34), were used as tumorigenic cancer cells (35-38). These cell lines were expanded in complete media [medium suggested for each cell line by the ATCC, 10% FBS (Asia Bioscience Co., Ltd.) and 1X antibiotic/antimycotic solution (cat. no. 15240-062; Thermo Fisher Scientific, Inc.)] in a humidified chamber with 95% air and 5% CO_2 at 37˚C with some exceptions. Briefly, four cell lines (FHC, T84, HCT116 $p53^{+/+}$ and HCT116 $p53^{-/-}$) were cultured with DMEM (cat. no. 12800-017; Thermo Fisher Scientific, Inc.) whereas three cell lines (CCD-18Co, LS 174T and Caco-2) were cultured with MEM (cat. no. 41500-034; Thermo Fisher Scientific). In addition, SW480 and SW620 cell lines were cultured with Leibovitz's L-15 medium (cat. no. 11415-064; Thermo Fisher Scientific, Inc.) supplemented with 10% FBS and 1X antibiotic/antimycotic solution, but maintained under 100% atmospheric air (without CO_2) in a humidified incubator at 37˚C.

To measure the expression of CSE1L in cells after treatment with 5-fluouracil (5-FU; cat. no. F6627; Merck KGaA) or sodium buyrate (NaB; cat. no. B5887; Merck KGaA), a total of $5x10^5$ cells were cultured for 24 h at 37˚C and before chemicals were added as follows: HCT116 $p53^{+/+}$ cells with 5-FU (40 μM) for 24 h at 37˚C, whereas HCT116 $p53^{-/-}$, SW480 and SW620 cells with NaB (5 mM) for 24 or 48 h at 37˚C.

To differentiate Caco-2 cells into a polarized enterocyte-like monolayer, cells were seeded at $8x10^5$ cells per well and cultured to confluence for 21 days at 37˚C, with changes of fresh MEM supplemented with 20% FBS and 1% antibiotic/antimycotic solution every 1-2 days (39,40).

Lentiviral knockdown of p53 and CSE1L. All lentiviral particles were obtained from the RNA Technology Platform and Gene Manipulation Core (https://rnai.genmed.sinica.edu.tw/index.html). Briefly, lentiviral particles were packaged in 293T cells (cat. no. CRL-3216; ATCC) using the 2nd generation system, with the combined ratio of lentiviral construct, packaging plasmid and envelope plasmid at 1 μg: 900 ng:100 ng. The 293T cells were then cultured in DMEM supplemented with 10% FBS and 0.1X antibiotic/antimycotic solution in a humidified chamber with 95% air and 5% CO_2 at 37˚C for 40 h. The cultured media were spun (300 x g for 5 min) to remove any packaging cells and supernatant containing viral paricles were collected. In total, two lentiviral constructs, namely pLKO.1_p53 (clone ID: TRCN0000003753) encoding a short hairpin RNA (shRNA) targeting p53 (shp53) and pLKO.1_CSE1L (clone ID: TRCN0000061789) targeting CSE1L (shCSE1L), were used for p53 knockdown in HCT116 $p53^{+/+}$ cells and CSE1L knockdown in HCT116 $p53^{-/-}$ cells. The control pLKO.1-luciferase (Luc; clone ID: TRCN0000072249) vector targeting Luc was used as the negative control (shLuc-HCT116 $p53^{+/+}$ for shp53 or shLuc-HCT116 $p53^{-/-}$ for shCSE1L). A total of $1.25x10^5$ cells/well were cultured in six-well plates for 24 h at 37˚C, before subsequent lentiviral infections (multiplicity of infection, 3) were performed to knock down the expression of target genes in the cells. Subsequently, medium containing 2 mg/ml puromycin (Thermo Fisher Scientific, Inc.) was used to select and maintain the stable clones. After a 48-h incubation at 37˚C, transfection efficiency was determined using reverse transcription-quantitative PCR (RT-qPCR).

RNA isolation, cDNA synthesis and gene quantitation. Total RNA was extracted from the parental CRC cell lines (CCD-18Co, FHC, LS 174T, T84, Caco-2, HCT116 $p53^{+/+}$, HCT116 $p53^{-/-}$, SW480 and SW620) and their derived cells, using the Easy Pure Total RNA Spin kit (cat. no. RT050; Bioman Scientific, Co., Ltd.) according to the manufacturer's protocol. Single-stranded cDNA was generated from 1 μg total RNA in the presence of an oligo $(dT)_{12}$ primer using the High-Capacity cDNA Reverse Transcription kit (cat. no. 4368813; Thermo Fisher Scientific, Inc.) according to the manufacturer's protocol. mRNA expression levels were quantified through qPCR using the LightCycler® TaqMan Master mix (cat. no. 04535286001; Roche Diagnostics GmbH) with a specific thermocycling profile (95˚C for 10 min, followed by 50 cycles at 95˚C for 10 sec and 60˚C for 20 sec) as described in a previous study (10,17). Primer sequences and probe numbers were CSE1L (Universal Probe: #27): forward, 5'-GTTGTCTACCGCCTGTCCA-3' and reverse, 5'-AAA TGCAGTTTAAAGCAGTGTCA-3'; c-Myc (Universal Probe: #34): forward, 5'-CACCAGCAGCGACTCTGA-3' and reverse, 5'-ACTCTGACCTTTTGCCAGGA-3'; p53 (Universal Probe: #12): forward, 5'-AGGCCTTGGAACTCAAGGAT-3' and reverse, 5'-CCCTTTTTGGACTTCAGGTG-3' and GAPDH (Universal Probe: #60): forward, 5'-CTCTGCTCCTCCTGT TCGAC-3' and reverse 5'-ACGACCAAATCCGTTGACTC-3'. Expression levels were quantified using the $2^{-\Delta\Delta Cq}$ method and normalized to the expression level of GAPDH (41). The human reference cDNA (HRC; cat. no. 636692; Takara Bio, Inc.) was used as an expression control. Gene expression data were obtained after performing ≥ three independent experiments with similar results.

Preparation of whole cell extracts and nuclear/cytosol fractions for western blotting. Whole-cell extracts from shLuc-HCT116 $p53^{-/-}$ and shCSE1L-HCT116 $p53^{-/-}$ cells were prepared using PRO-PREP Protein Extraction Solution (Intron Biotechnology, Inc.) in the presence of a protease inhibitor (cat. no. P8340; Merck KGaA) according to the manufacturer's protocols. Cell fractionation was performed using NE-PER Nuclear and Cytoplasmic Extraction Reagents kit (cat. no. 78833; Thermo Fisher Scientific, Inc.) to isolate the different protein fractions from the cytoplasm and nuclei, according to the manufacturer's protocols. The purity of non-nuclear and nuclear fractions was determined using specific protein markers, namely Tubulin and TATA-box binding protein (TBP), respectively. Each protein concentration was then determined using a Bio-Rad Protein Assay reagent

(cat. no. 500-0006; Bio-Rad Laboratories, Inc.). Next, 30 μg of protein per lane was denatured at 95˚C for 10 min, separated using 12% SDS-PAGE in 1X NuPAGE LDS Sample Buffer (Thermo Fisher Scientific, Inc.) and then transferred onto 0.2-μm PolyScreen 2 PVDF Transfer membranes (PerkinElmer, Inc.). The membranes were blocked with 3% bovine serum albumin (cat. no. ALB001.100; BioShop Canada, Inc.) for 1 h at room temperature and incubated with the following primary antibodies for 1 h at room temperature: Anti-CSE1L (1:1,000; cat. no. 22219-1-AP; Proteintech Group, Inc.), anti-p53 (1:500; cat. no. NCL-L-p53-DO7; Leica Biosystems, Inc.), anti-cyclin A2 (CCNA2; 1:2,000; cat. no. 4656P; Cell Signaling Technology, Inc.), anti-cyclin B2 (CCNB2; 1:2,000; cat. no. ab185622; Abcam), anti-cyclin D1 (CCND1; 1:1,000; cat. no. 2978; Cell Signaling Technology, Inc.), anti-tubulin (1:1,000; cat. no. sc-5286, Santa Cruz Biotechnology, Inc.), anti-TBP (1:1,000; cat. no. 22006-1-AP, Proteintech Group, Inc.) and anti-GAPDH (1:5,000; cat. no. 60004-1-Ig; Proteintech Group, Inc.). Expression of GAPDH was used as the endogenous control gene. After incubation of the primary antibodies, the membranes were incubated with a HRP-conjugated anti-mouse IgG (H&L) secondary antibody (1:5,000; cat. no. ab6808; Abcam) HRP-conjugated antirabbit IgG secondary antibody (1:5,000; cat. no. L3012; Signalway Antibody LLC) for 60 min at room temperature. Protein bands were visualized using Western Lightning Chemiluminescence Reagent Plus (PerkinElmer, Inc.) and an AlphaView software (version 3.2.2) of the FluorChem FC2 Imaging System (Cell Biosciences, Inc.) according to the manufacturers' protocols (Alpha Innotech FluorChem FC2 Imaging System; Cell Biosciences, Inc.).

Cell cycle analysis and immunofluorescent staining. shLuc-HCT116 $p53^{-/-}$ cells and shCSE1L HCT116 $p53^{-/-}$ cells were starved under low-serum conditions (0.5%) for 24 h at 37˚C and then cultured in complete medium for 24 h at 37˚C. They were then fixed in 70% prechilled ethanol for >1 h at -20˚C, washed twice with PBS, incubated with 1 μg/ml RNase A for 1 h at 37˚C and stained with 5 μg/ml propidium iodide for 1 h at room temperature. Light emission at 585 nm from propidium iodide-stained nuclei was detected using a BD FACScan flow cytometer (BD Bioscienes). The percentages of cells (from $1x10^4$ cells) at different phases of cell cycle were determined using FlowJo software (v. 8.7; FlowJo LLC).

A total of $1.5x10^4$ HCT116 $p53^{-/-}$ cells and HCT116 $p53^{+/+}$ cells for immunofluorescence staining were cultured on 12-mm cover slips (SPL Life Sciences). The cells were probed with a diluted anti-CSE1L antibody (1:50; cat. no. 22219-1-AP; Proteintech Group, Inc.) or anti-Tubulin antibody (1:50; cat. no. sc-5286; Santa Cruz Biotechnology, Inc.) for 16 h at 4˚C after fixation with 4% paraformaldehyde (Merck KGaA) in PBS for 10 min at room temperature, permeabilization with 0.1% Triton X-100 (Merck KGaA) in PBS for 35 min at room temperature, and blocking with 1.5% normal horse serum blocking solution (cat. no. S-2000-20; Vector Laboratories, Inc.; Maravai LifeSciences) in 10 ml PBS for 30 min at room temperature. Next, the FITC-conjugated secondary antibody (1:200; cat. no. AP132F; Merck KGaA) for CSE1L and the Cy3-conjugated secondary antibody (1:200; cat. no. AP124C; Merck KGaA) for α-tubulin were incubated for 1 h at room temperature. Nuclear DNA was stained with 1 μg/ml DAPI (cat. no. 71-03-01; Kirkegaard & Perry Laboratories Inc.) for 15 min at room temperature. The stained samples were dehydrated through an ascending ethanol series and air-dried for 10 min at room temperature before being mounted in VECTASHIELD® HardSet™ Antifade Mounting Medium (cat. no. H-1400; Vector Laboratories, Inc.; Maravai LifeSciences). They were then observed using a Nikon Eclipse 80i fluorescence microscope at x200 magnification (Nikon Corporation) before fluorescence was quantified from > five fields of views (10 views for HCT116 $p53^{+/+}$ cells and five views for HCT116 $p53^{-/-}$ cells) using Adobe Photoshop (version CS6; Adobe Systems, Inc.).

Immunohistochemical staining for mouse tissues. Mouse colorectal samples were fixed with 4% paraformaldehyde in PBS for 10 min at room temperture and embedded in paraffin. Paraffin sections (3-5 μm thickness) were obtained and then processed using the avidin-biotin-immunoperoxidase method to measure the expression of CSE1L and p53. Immunohistochemical staining was performed on an automated BenchMark GX slide stainer (Roche Diagnostics) in a closed and fixed program, which included deparaffinization with EZ Prep solution (cat. no. 950-102; Ventana Medical Systems) at 75˚C for 8 min, antigen retrieval with Cell Conditioning 1 solution (cat. no. 950-124; Ventana Medical Systems) at 95˚C for 64 min, incubation with primary antibody (at 37˚C for 32 min) followed by HQ Universal Linker (cat. no. 253-4580; Ventana Medical Systems) at 37˚C for 8 min and HRP Multimer (cat. no. 253-4581; Ventana Medical Systems) at 37˚C for 8 min and visualization by DAB. The Optiview DAB IHC detection kit (cat. no. 760-700; Roche Diagnostics) was used as a detection system. All sections were counterstained with Hematoxylin II at 25˚C for 8 min (cat. no. 790-2208; Ventana Medical Systems) and Bluing Reagent at 25˚C for 4 min (cat. no. 760-2037; Ventana Medical Systems). Anti-CSE1L (1:50; cat. no. 22219-1-AP; Proteintech Group, Inc.) or anti-p53 (1:50; cat. no. BS-8687R, Thermo Fisher Scientific, Inc.) were hybridized to detect target protein. A pathologist (CYL) observed and categorized the immunohistochemically stained sections using a Nikon Eclipse 80i fluorescence microscope at x200 magnification by light microscopy (Nikon Corporation).

Cell migration assay. The shLuc-HCT116 $p53^{-/-}$ and shCSE1L-HCT116 $p53^{-/-}$ cells were grown to confluence on six-well plates before a wound was made by scraping across the cell monolayer with a 30 gauge needle (outer diameter, 300 μm). The motility of the cells at the edge of a scratch wound in the presence or absence of NaB (5 mM) was then analyzed. Cells at the wound edge were imaged using a bright-field/phase-contrast microscope at x200 magnification. Repeat images were taken after wounding in medium with low serum (DMEM, 1% FBS and 1% antibiotic/antimyotic solution) at 37˚C for 16 h and followed with complete media for indicated time (0, 4 and 8 h). Serum-free media was first tested for this assay but HCT $p53^{-/-}$ cells could not survive in this condition, which necesitated the use of 1% for maintenance followed by complete medium (10% FBS) for the assay. It is predicted that the extent of interference due to cell proliferation would be

minimal, as the doubling time of HCT116 cells is ~18 h and the maximum duration of the wound healing assay in the present study was 8 h. ImageJ (version 1.45s; National Institutes of Health) was used to measure the migration distance at each time point (42). Next, the cell migration efficiency after 8 h of cultivation was assessed using the recovery ratio according to the reduction of wound area (the percentage of cell area difference, relative to the inititial time point of 0 h) (43). In total, three or four independent sets of experiments were performed for each assay.

Statistical analysis. The difference in gene expression, cell phase and cell migration between the groups was assessed. A unpaired student's t test was used to compare two groups whereas one-way analysis of variance was performed to compare among ≥ three different groups. All ANOVA analyses were followed with Bonferroni post hoc testing. The statistical analyses were performed using SPSS (v. 22.0; IBM Corp). Data are presented as the mean ± standard error of the mean. $P<0.05$ was considered to indicate a statistically significant difference.

Results

CSE1L mRNA expression levels in the different colonic and CRC cell lines. The expression levels of CSE1L in different colonic and CRC cell lines were quantified (Fig. 1). CSE1L expression levels in the two non-transformed cell lines, CCD-18Co and FHC, varied significantly according to their different p53 mutation statuses (Fig. 1A). Briefly, the CCD-18Co cells with the wild-type p53 expressed the lower levels of CSE1L compared with those in FHC cells with the R273H p53 mutant. Among the CRC cell lines, Caco-2 cells haboring p53 mutations exhibited significantly higher CSE1L expression levels compared with those in LS 174T and T84 cells, both of which express wild-type p53 (Fig. 1B). However, CSE1L and c-Myc mRNA expression levels both simulataneously and progressively reduced in Caco-2 cells as their confluency increased (Fig. 1C and D). In addition, the protein expression levels of CSE1L and c-Myc were markedly decreased in Caco-2 cells following proliferation to confluence on day 21 compared with those in cells on day 1 (Fig. 1E).

Higher CSE1L protein expression levels were also observed in HCT116 cells not expressing p53 (Fig. 1F and G) or in HCT116 cells following p53 knockdown (Fig. 1H and I). Compared with those in HCT116 $p53^{+/+}$ cells, either mRNA (Fig. 1F) or protein (Fig. 1G) expression levels of CSE1L were markedly higher in HCT116 $p53^{-/-}$ cells. This differential expression was also observed in HCT116 $p53^{+/+}$ cells with p53 expression knocked down. After p53 was significantly knocked down in HCT116 $p53^{+/+}$ cells compared with that in shLuc-transfected cells (Fig. 1H), the expression level of CSE1L mRNA was also significantly increased (Fig. 1I). A similar finding could also be made on p53 protein expression in HCT116 $p53^{+/+}$ cells after 5-FU (40 μM) treatment for 24 h, which was increased (Fig. 1J). In addition, the expression of CSE1L was markedly reduced in the 5-FU-treated HCT116 $p53^{+/+}$ cells compared with that in their untreated counterparts (Fig. 1J).

Cell cycle regulation of p53-null CRC cells by CSE1L expression. To understand the molecular significance of CSE1L expression in CRC cells, CSE1L expression was knocked down in HCT116 $p53^{-/-}$ cells, which was achieved to significant levels compared with that in the shLuc-HCT116 $p53^{-/-}$ cells (Fig. 2A). In addition, shCSE1L-HCT116 $p53^{-/-}$ cells expressed markedly lower expression levels of CSE1L protein (Fig. 2B). Compared with those in shLuc-HCT116 $p53^{-/-}$ cells, the cell populations in various phases of cell the cycle were altered in the shCSE1L-HCT116 $p53^{-/-}$ cells (Fig. 2C). Specifically, the percentage of shCSE1L-HCT116 $p53^{-/-}$ cells in S phase was significantly decreased, whereas that in the G_1 and G_2/M phases was significantly increased, compared with those of shLuc-HCT116 $p53^{-/-}$ cells (Fig. 2C and D). Supporting this, shCSE1L-HCT116 $p53^{-/-}$ cells also expressed markedly lower protein levels of cell cycle regulators CCNA2, CCNB2 and CCND1 compared with those in shLuc-HCT116 $p53^{-/-}$ cells (Fig. 2E).

Dynamic expression of CSE1L in HCT116 CRC cells during mitosis. Analysis of CSE1L expression during different phases of mitosis in HCT116 cells revealed that expression profile of CSE1L changed dynamically throughout mitosis (Fig. 3). Both HCT116 $p53^{-/-}$ cells and HCT116 $p53^{+/+}$ cells expressed high levels of CSE1L at prophase and metaphase. However, the signals for CSE1L in HCT116 $p53^{-/-}$ cells were stronger compared with those in HCT116 $p53^{+/+}$ cells during interphase and cytokinesis. As shown in Fig. 3A for HCT116 $p53^{-/-}$ cells, CSE1L emerged at interphase, increased at prophase, peaked during metaphase before declining at the cytokinesis stage. The dynamic expression profiles of CSE1L in HCT116 $p53^{-/-}$ cells during mitosis was subsequently analyzed, with the highest levels of CSE1L expression found at prophase and metaphase (Fig. S1). By contrast, as shown in Fig. 3B, low levels of CSE1L expression were detected during interphase and cytokinesis in HCT116 $p53^{+/+}$ cells, which increased markedly at prophase before peaking at metaphase.

Reduced CSE1L expression in butyrate-treated HCT116 $p53^{-/-}$ cells and colon tumors in mice treated with B. pullicaecorum administration. HCT116 $p53^{-/-}$ cells treated with 5 mM NaB for 24 h exhibited lower expression levels of of both CSE1L mRNA (Fig. 4A) and protein in the total cell lysate (Fig. 4B) compared with those in cells not treated with NaB. In addition, NaB treatment reduced the mRNA expression of CSE1L in both the SW480 and SW620 cell lines (with the p53 mutant) after 24 and 48 h (Fig. S2). In the cytosolic and nuclear compartments of HCT116 $p53^{-/-}$ cells, the expression levels of CSE1L also decreased as a result of 5 mM NaB treatment (Fig. 4B). Furthermore, the recovery ratio in the migration of shCSE1L-HCT116 $p53^{-/-}$ or NaB-treated-shLuc-HCT116 $p53^{-/-}$ cells was significantly decreased compared with that in the control shLuc-HCT116 $p53^{-/-}$ cells (Fig. 4C and D).

CSE1L expression in colon tumors of mice with B. pullicaecorum administration. H&E staining and immunohistochemical analysis of p53 and CSE1L expression was performed in the mouse intestinal tissues. Reactivity was almost absent in control healthy intestinal tissues (Fig. 5). Compared with those in the control mice, colon tumors were induced in mice by DMH/DSS treatment (Fig. 5). In

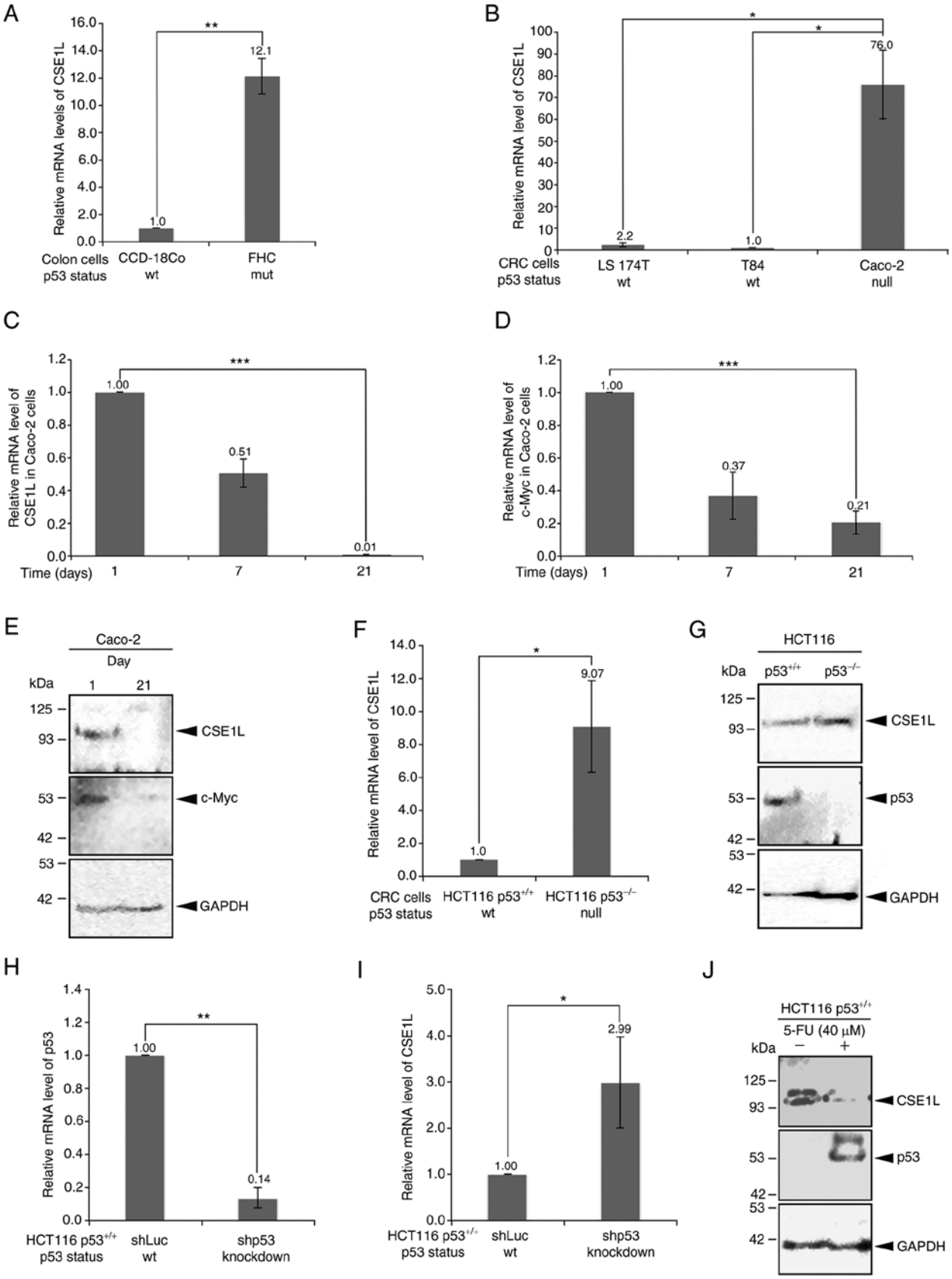

Figure 1. Different CSE1L expression levels in the colon cell lines. (A) Relative mRNA expression levels of CSE1L in CCD-18Co and FHC cells. (B) Relative mRNA expression levels of CSE1L in the CRC cell lines. (C) Relative mRNA expression levels of CSE1L in overconfluent Caco-2 cells. (D) Relative mRNA expression levels of c-Myc in overconfluent Caco-2 cells. (E) Protein expression level of CSE1L and c-Myc in overconfluent Caco-2 cells. (F) Relative mRNA expression levels of CSE1L in HCT116 cells with or without p53 expression. (G) Protein expression level of CSE1L in HCT116 cells with or without p53 expression. (H) Knockdown efficacy of p53 by mRNA level in HCT116 $p53^{+/+}$ cells. (I) Relative mRNA expression levels of CSE1L in HCT116 cells without or with p53 knockdown. (J) Protein expression levels of CSE1L in 5-FU-treated wild-type HCT116 cells. *P<0.05, **P<0.01 and ***P<0.001. CRC, colorectal cancer; 5-FU, 5-fluouracil; shLuc, lentiviral construct targeting luciferase; shp53, lentiviral construct targeting p53; wt, wild-type; sh, short hairpin; CSE1L, chromosome segregation 1-like protein.

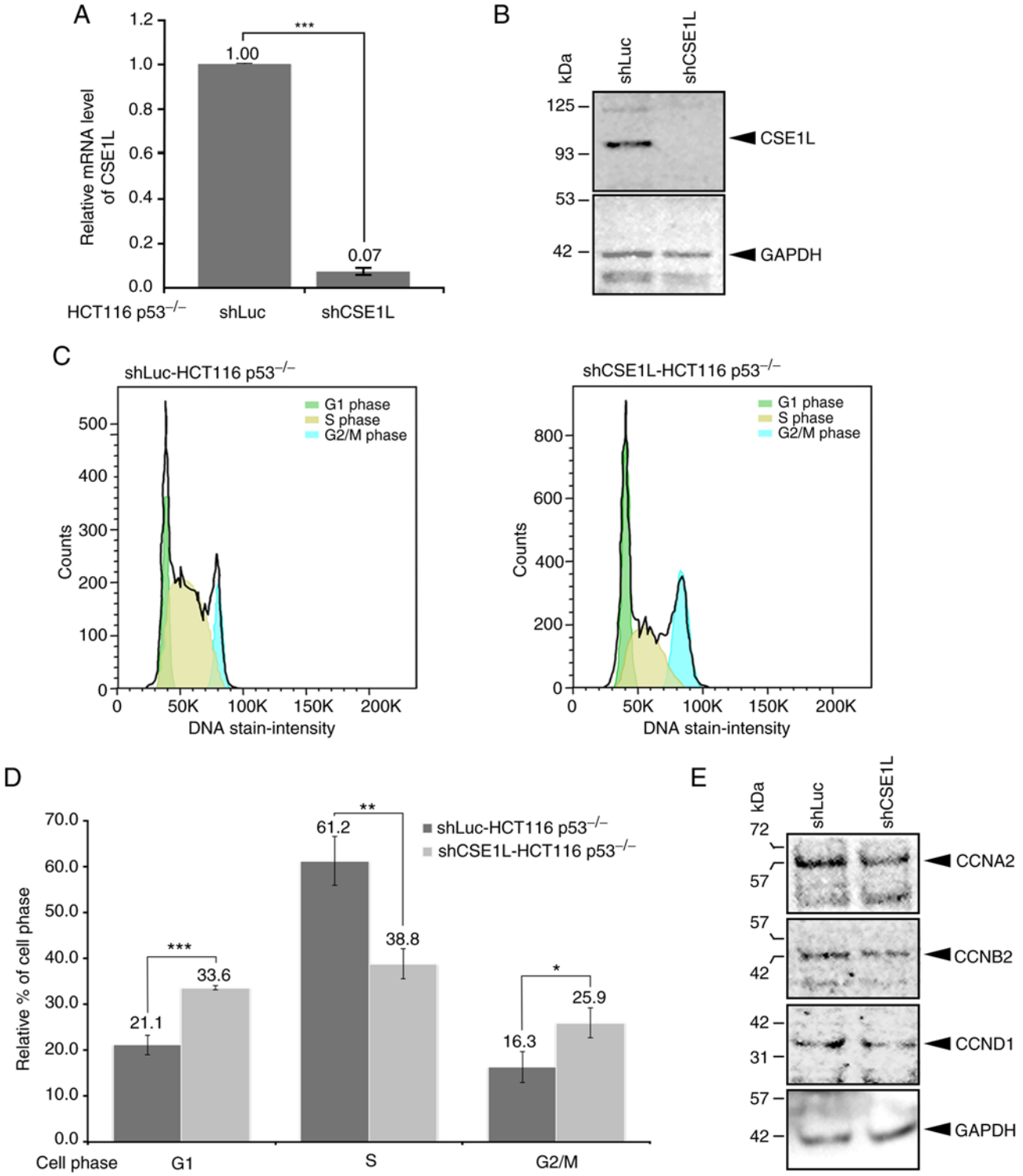

Figure 2. Cellular changes in HCT116 p53$^{-/-}$ cells after knocking down CSE1L expression. (A) Knockdown efficacy of CSE1L in HCT116 p53$^{-/-}$ cells. (B) Protein expression levels of CSE1L in HCT116 p53$^{-/-}$ cells without or with CSE1L knockdown. (C) Population of HCT116 p53$^{-/-}$ cells in the various phases of cell cycle without or with CSE1L knockdown. (D) Percentages of shCSE1L-HCT116 p53$^{-/-}$ cells in the various phases of cell cycle without or with knockdown of CSE1L expression were quantified. (E) Protein expression levels of CCNA2, CCNB2 and CCND1 in HCT116 p53$^{-/-}$ cells without or with CSE1L knockdown. *P<0.05, **P<0.01 and ***P<0.001. HCT116 p53$^{-/-}$, p53-null HCT116 cells. shLuc, lentiviral construct targeting luciferase; shCSE1L, lentiviral construct targeting CSE1L; sh, short hairpin; CSE1L, chromosome segregation 1-like protein; CCNA2, cyclin A2; CCNB2, cyclin B2; CCND1, cyclin D1.

the colons of mice following DMH/DSS treatment without *B. pullicaecorum* administration, histological sections showed exophytic tumors exhibiting irregular and complex dysplastic glands, indicating intramucosal adenocarcinoma (red arrows in the middle panel of Fig. 5). Weak nuclear staining of p53 and increased expression of CSE1L were observed in large tumors with high-grade dysplasia (Fig. 5). By contrast, in mouse tissues treated with *B. pullicaecorum*, the histological sections revealed polypoid lesions consisting mostly of low-grade adenomas, representing the early stage of neoplasia

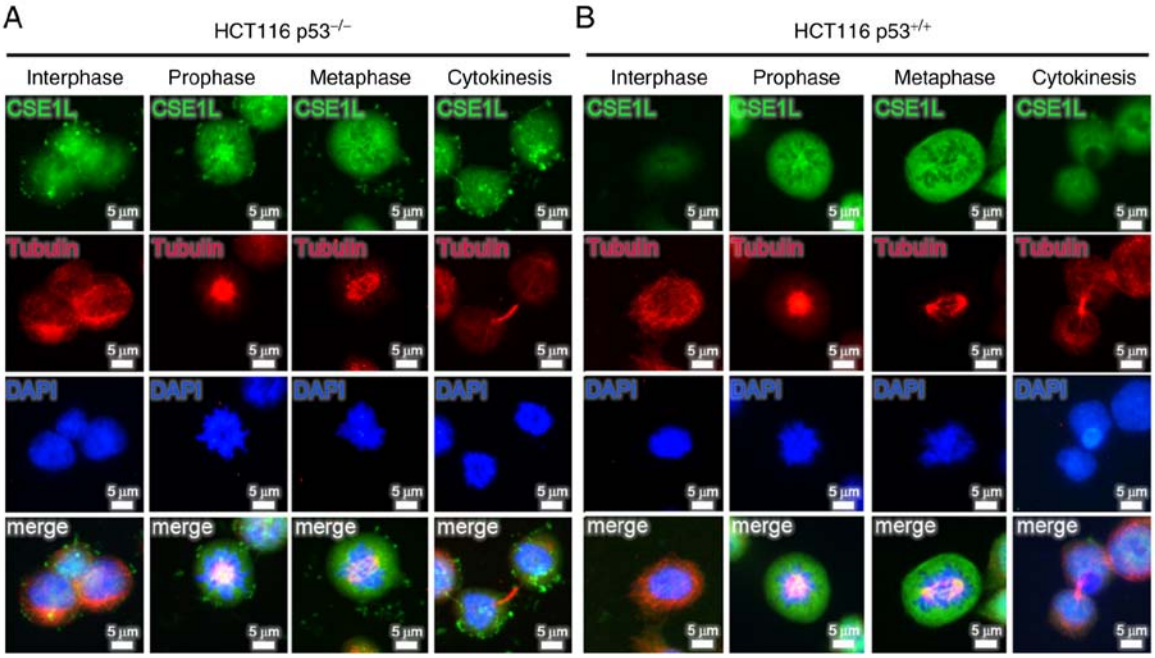

Figure 3. Dynamic expression profiles of CSE1L throughout the mitotic phase of the cell cycle in HCT116 cells of different p53 statuses. Immunofluorescence microscopy was used to evaluate the localization of endogenously expressed CSE1L in separate (A) HCT116 $p53^{+/+}$ cells and (B) HCT116 $p53^{-/-}$ cells at distinct phases of mitosis. CSE1L are presented in green. DAPI (nuclear DNA) is presented in blue. Tubulin is presented in red. Merge represents CSE1L + Tubulin + DAPI. Scale bar, 5 μm. HCT116 $p53^{-/-}$, p53-null HCT116 cells; CSE1L, chromosome segregation 1-like protein.

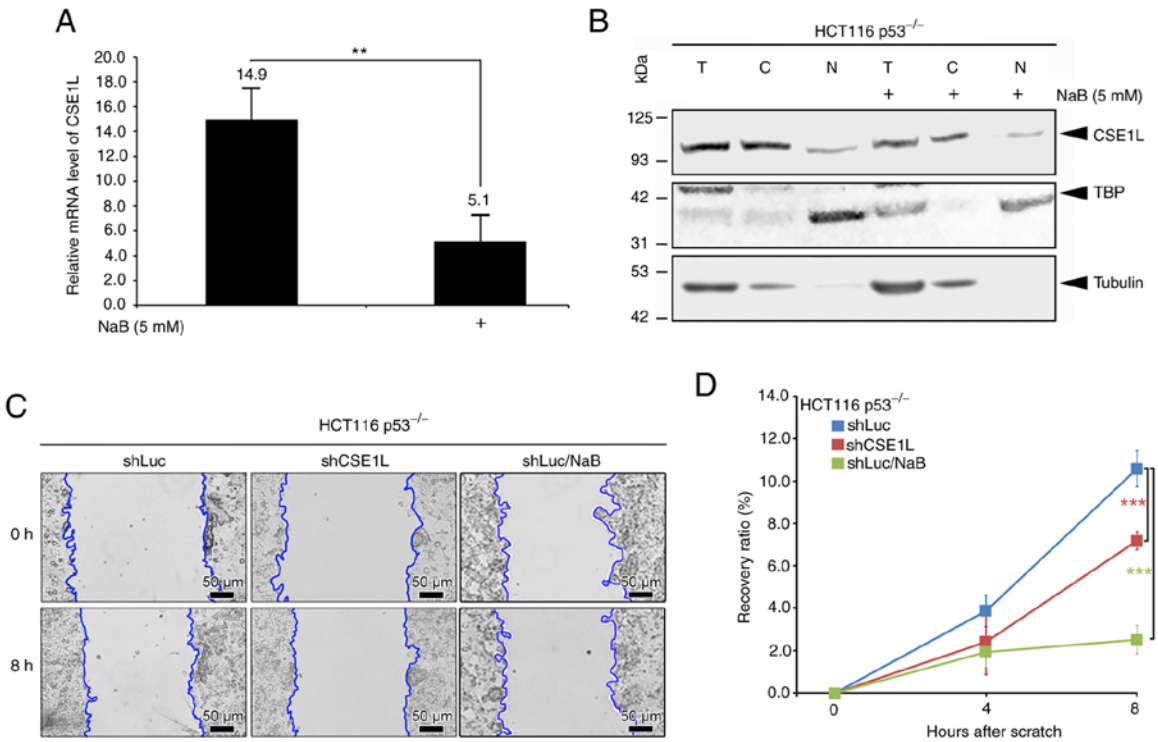

Figure 4. Effects of butyrate on CSE1L expression in HCT116 $p53^{-/-}$ cells. (A) Relative mRNA expression levels of CSE1L in cells without or with butyrate treatment. (B) Protein expression levels of CSE1L in the nucleus or cytosol of cells following butyrate treatment. (C) Migration changes and (D) Recovery ratios of cells without or with CSE1L knockdown or butyrate treatment. Blue line presents the edge of cell migration. Scale bars, 50 μm. **P<0.01 and ***P<0.001. CSE1L, chromosome segregation 1-like protein; TBP, TATA-binding protein; NaB, sodium butyrate; T, total cell lysate; C, cytosolic part; N, nuclear part; shLuc, lentiviral construct targeting luciferase; shCSE1L, lentiviral construct targeting CSE1L; sh, short hairpin.

(red arrows in the right panel of Fig. 5). Immunohistochemical analysis showed positive nuclear staining for p53 and a low intensity CSE1L signal were detected in precancerous tumors with low-grade dysplasia from DMH/DSS-treated mice that were administered with butyrate-producing *B. pullicaecorum* through oral gavage.

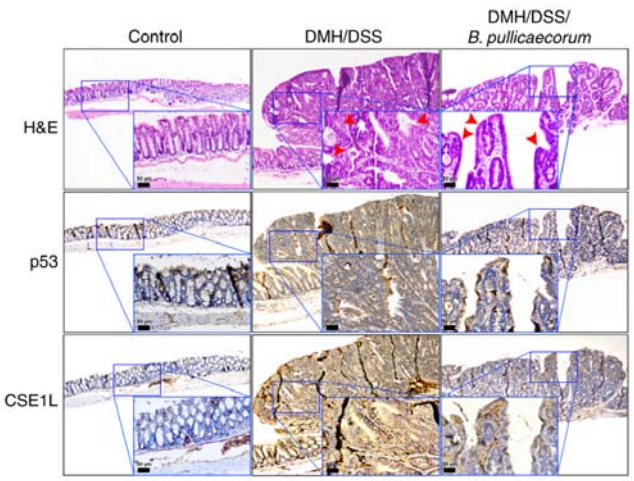

Figure 5. Representative immunohistochemical staining images for the expression of p53 and CSE1L proteins in the colon tissues. Colon tissues were sectioned from the following different groups: Control group, consisting of mice that did not receive any chemical treatment or *B. pullicaecorum* administration; DMH/DSS group, consisting of mice that received DMH through intraperitoneal injection and DSS in their drinking water but did not receive *B. pullicaecorum*; and DMH/DSS/*B. pullicaecorum* group, consisting of mice that received DMH/DSS and *B. pullicaecorum*. Colon tumors exhibited weak nuclear staining of p53 and markedly increased expression of CSE1L. Insets show the magnified views of the boxed areas. Red arrows indicate the intramucosal adenocarcinoma in DMH/DSS group (middle panel) and the low-grade adenoma in DMH/DSS/*B. pullicaecorum* group (right panel). Scale bar, 50 μm for inset. CSE1L, chromosome segregation 1-like protein; DMH, 1,2-dimethylhydrazine; DSS, dextran sulphate sodium; *B. pullicaecorum*, *Butyricicoccus pullicaecorum*.

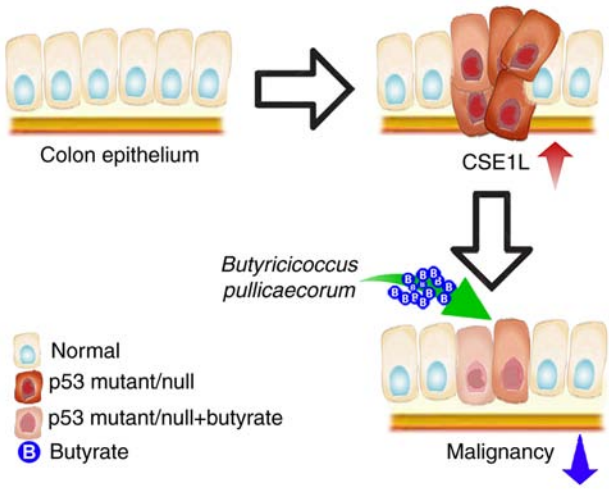

Figure 6. Effect of butyrate supplementation and CSE1L overexpression on the genetic distortion caused by p53 mutations in colorectal cancer. Butyrate supplementation downregulates expression of CSE1L in p53-mutated CRC cells to mitigate the maligancy of CRC. CSE1L, chromosome segregation 1-like protein.

Discussion

CSE1L overexpression was previously found to associate with the progression of a number of gastrointestinal cancers, including esophageal cancer, gastric cancer, hepatocellular carcinoma and CRC (1,2,44,45). Furthermore, CSE1L can promotes the nuclear distribution of the transcriptional coactivator with PDZ-binding motif to enhance the malignancy of human cancer tissues from osteosarcoma, glioma and lung cancer (46). Therefore, understanding the molecular mechanism underlying the effects of CSE1L may facilitate the optimization of cancer therapy (47).

CSE1L and p53 serve antagonistic effects on cell cycle regulation (6,48). In CRC, whilst ~50% all samples harbor p53 mutations that have been shown to be associated with poor prognosis and chemoresistance (49,50), others have reported that the majority of CRC tissues are positive for CSE1L expression (4,8,9). In the present study, in the colon cell lines tested, which were either cells from the normal colon or from cancer tissues, they were found to express varing levels of CSE1L. The colon cell lines haboring mutant p53 proteins (FHC and Caco-2) exhibited relatively high CSE1L expression levels. In addition, p53-null HCT116 cells or HCT116 cells with p53 expression knocked down were found to express higher levels of CSE1L. Conversely, an overexpression of wild-type p53 in CRC cells by 5-FU treatment reduced CSE1L expression. These results provide evidence that changing the functionality of p53 in CRC cells can alter the expression of CSE1L.

Overexpression of CSE1L in CRC has been associated with tumor development and malignancy (8,51,52), such that CSE1L knockdown can inhibit the growth and metastasis of CRC tumors (2,53). Pimiento *et al* (8) previously reported that CSE1L knockdown may represent a potential target for CRC treatment. This finding is consistent with that in the present study. Differentiation of Caco-2 cells into a polarized enterocyte-like monolayer was shown reduce the extent of malignancy (39). Decreasing CSE1L expression levels were accompanied by reduced c-Myc expression as the confluency of Caco-2 cells increased. In addition, CSE1L knockdown in HCT116 $p53^{-/-}$ cells, specifically shCSE1L-HCT116 $p53^{-/-}$ cells in the present study, was found to arrest cell cycle progression at the G_1 phase whilst inhibiting DNA replication at S phase. These results would agree with immunofluorescent images of cells under different mitotic phases, which indicated that the CSE1L-expressing HCT116 $p53^{-/-}$ cells would potentiate the expression of CSE1L at prophase and metaphase. A lack of CSE1L upregulation in the HCT116 $p53^{-/-}$ cells, such as shCSE1L-HCT116 $p53^{-/-}$ cells or butyrate-treated HCT116 $p53^{-/-}$ cells, thereby impeded CRC cell cycle progression or migration. Depletion of cyclins caused by CSE1L knockdown also suggested that the cell cycle was arrested at the G_1 phase. As previously reported by Ye *et al* (49) in breast cancer cells, this form of cell cycle arrest may not be only caused by reduced cyclin expression but also by the upregulated expression of the cytochrome P450 family of proteins (54). It will be necessary to examine the expression of the cytochrome P450 superfamily of proteins in the different CRC cell lines following the manipulation of CSE1L expression to clarify the significance of this relationship. Taken together, results from the present study imply that CSE1L knockdown can impede CRC progression. Since CSE1L has been reported to be a potential target for CRC treatment (8,55), methods that can decrease the expression of CSE1L in CRC may serve clinical potential.

Butyrates can regulate intestinal barrier function and has potential clinical application for human gastrointestinal diseases (10,56,57). In addition, it has been applied in

combination with other chemotherapeutic agents, such as irinotecan, for CRC treatment (23). In the present study, the expression of CSE1L was reduced after the treatment of CRC cells with butyrate *in vitro*) or after the administration of the butyrate-producing *B. pullicaecorum* to CRC-bearing mice *in vivo*). Butyrate also reduced the CSE1L expression levels in CRC cells carrying p53 mutations, such as SW480 cells and SW620 cells. Therefore, butyrate may also display anticancer properties by downregulating the expression of CSE1L, in addition to butyrate also exhibiting synergistic anticancer effects with p53 (58,59). In combination with the present results, CSE1L knockdown may mitigate CRC malignancy and that butyrate may reduce the expression of CSE1L further.

In the present study, the results demonstrated that butyrate could reduce the expression of CSE1L in CRC cells in not only the *in vitro* cell modesl, but also an *in vivo* animal model. Administration of *B. pullicaecorum* was previously shown to improve the clinical outcome of CRC and colitis (17,26). Tumors with more intense nuclear staining of p53 and weaker CSE1L staining were especially found in mice bearing DMH/DSS-induced CRC that were administered with *B. pullicaecorum*. Pathologically, these tumors were diagnosed to be precancerous with low-grade dysplasia. However, the present study may not have completely elucidated the precise mechanism by which *B. pullicaecorum* regulates CSE1L expression or how the differential CSE1L expression can arrest cell cycle progression in CRC. In the future, a further *in vivo* study is required to evaluate the prognosis of mice with CSE1L overexpression after *B. pullicaecorum* administration.

In conclusion, high CSE1L expression levels is associated with the malignancy of CRC, where reduced CSE1L expression in CRC cells may hinder proliferation or improve cancer outcomes. As depicated in Fig. 6, CSE1L represents a potential target for CRC treatment, such that the reduction of CSE1L expression or activity can be achieved by butyrate treatment or *B. pullicaecorum* administration. This is because butyrate can repress CSE1L-induced tumorigenic potential, whereby butyrate-producing microbes, such as *B. pullicaecorum*, may reverse the genetic distortion caused by p53 mutations in CRC by regulating CSE1L expression. Therefore, CSE1L-induced CRC growth may be impaired by butyrate supplementation or *B. pullicaecorum* administration.

Acknowledgements

Not applicable.

Funding

The present study was supported by grants from the Cathay General Hospital and Taipei Medical University (grant nos. 106CGH-TMU-03 and 107CGH-TMU-02). The funders had no role in the study design, data collection and analysis, decision to publish, or preparation of the manuscript.

Availability of data and materials

The datasets used and/or analyzed during the current study are available from the corresponding author on reasonable request.

Authors' contributions

CCC, RNY and CJH were involved in the study conception and design. HHS, YAK, PYL, CYL, KWC and CJH performed experiments and analysis of data. CCC, CJH, WYK, CYL and WCK were involved in the study conception and design, performing the experiments and analysis of data. RNY and CJH can confirm the authenticity of all the raw data. All authors read and approved the final manuscript.

Ethics approval and consent to participate

The animal experiment in this study was performed in accordance with the principles of replacement, refinement and reduction and were approved (approval no. 107-008) by the Institutional Animal Care and Use Committees of Cathay General Hospital (Taipei, Taiwan).

Patient consent for publication

Not applicable.

Competing interests

The authors declare that they have no competing interests.

References

1. Jiang K, Neill K, Cowden D, Klapman J, Eschrich S, Pimiento J, Malafa MP and Coppola D: Expression of CAS/CSE1L, the cellular apoptosis susceptibility protein, correlates with neoplastic progression in barrett's esophagus. Appl Immunohistochem Mol Morphol 26: 552-556, 2018.
2. Li Y, Yuan S, Liu J, Wang Y, Zhang Y, Chen X and Si W: CSE1L silence inhibits the growth and metastasis in gastric cancer by repressing GPNMB via positively regulating transcription factor MITF. J Cell Physiol 235: 2071-2079, 2020.
3. Liao CF, Lin SH, Chen HC, Tai CJ, Chang CC, Li LT, Yeh CM, Yeh KT, Chen YC, Hsu TH, *et al*: CSE1L, a novel microvesicle membrane protein, mediates Ras-triggered microvesicle generation and metastasis of tumor cells. Mol Med 18: 1269-1280, 2012.
4. Tai CJ, Su TC, Jiang MC, Chen HC, Shen SC, Lee WR, Liao CF, Chen YC, Lin SH, Li LT, *et al*: Correlations between cytoplasmic CSE1L in neoplastic colorectal glands and depth of tumor penetration and cancer stage. J Transl Med 11: 29, 2013.
5. Tunccan T, Duzer S, Dilek G, Yuksel UM, Cetiner H, Kılıc C, Ant A and Duran AB: The role of CSE1L expression in cervical lymph node metastasis of larynx tumors. Braz J Otorhinolaryngol 87: 42-46, 2021.
6. Tanaka T, Ohkubo S, Tatsuno I and Prives C: hCAS/CSE1L associates with chromatin and regulates expression of select p53 target genes. Cell 130: 638-650, 2007.
7. Liao CF, Luo SF, Shen TY, Lin CH, Chien JT, Du SY and Jiang MC: CSE1L/CAS, a microtubule-associated protein, inhibits taxol (paclitaxel)-induced apoptosis but enhances cancer cell apoptosis induced by various chemotherapeutic drugs. BMB Rep 41: 210-216, 2008.
8. Pimiento JM, Neill KG, Henderson-Jackson E, Eschrich SA, Chen DT, Husain K, Shibata D, Coppola D and Malafa M: Knockdown of CSE1L gene in colorectal cancer reduces tumorigenesis in vitro. Am J Pathol 186: 2761-2768, 2016.
9. Tai CJ, Hsu CH, Shen SC, Lee WR and Jiang MC: Cellular apoptosis susceptibility (CSE1L/CAS) protein in cancer metastasis and chemotherapeutic drug-induced apoptosis. J Exp Clin Cancer Res 29: 110, 2010.
10. Huang CC, Shen MH, Chen SK, Yang SH, Liu CY, Guo JW, Chang KW and Huang CH: Gut butyrate-producing organisms correlate to placenta specific 8 protein: Importance to colorectal cancer progression. J Adv Res 22: 7-20, 2020.

11. Wang Y, Huang D, Chen KY, Cui M, Wang W, Huang X, Awadellah A, Li Q, Friedman A, Xin WW, *et al*: Fucosylation deficiency in mice leads to colitis and adenocarcinoma. Gastroenterology 152: 193-205, 2017.
12. Venegas DP, De la Fuente MK, Landskron G, González MJ, Quera R, Dijkstra G, Harmsen HJM, Faber KN and Hermoso MA: Short chain fatty acids (scfas)-mediated gut epithelial and immune regulation and its relevance for inflammatory bowel diseases. Front Immunol 10: 277, 2019.
13. Puertollano E, Kolida S and Yaqoob P: Biological significance of short-chain fatty acid metabolism by the intestinal microbiome. Curr Opin Clin Nutr Metab Care 17: 139-144, 2014.
14. Gill PA, van Zelm MC, Muir JG and Gibson PR: Review article: Short chain fatty acids as potential therapeutic agents in human gastrointestinal and inflammatory disorders. Aliment Pharmacol Ther 48: 15-34, 2018.
15. Kannen V, Parry L and Martin FL: Phages enter the fight against colorectal cancer. Trends Cancer 5: 577-579, 2019.
16. Boesmans L, Valles-Colomer M, Wang J, Eeckhaut V, Falony G, Ducatelle R, Van Immerseel F, Raes J and Verbeke K: Butyrate producers as potential next-generation probiotics: Safety assessment of the administration of butyricicoccus pullicaecorum to healthy volunteers. mSystems 3: e00094-e00018, 2018.
17. Chang SC, Shen MH, Liu CY, Pu CM, Hu JM and Huang CJ: A gut butyrate-producing bacterium Butyricicoccus pullicaecorum regulates short-chain fatty acid transporter and receptor to reduce the progression of 1,2-dimethylhydrazine-associated colorectal cancer. Oncol Lett 20: 327, 2020.
18. Eeckhaut V, Wang J, Van Parys A, Haesebrouck F, Joossens M, Falony G, Raes J, Ducatelle R and Van Immerseel F: The probiotic butyricicoccus pullicaecorum reduces feed conversion and protects from potentially harmful intestinal microorganisms and necrotic enteritis in broilers. Front Microbiol 7: 1416, 2016.
19. Wu X, Wu Y, He L, Wu L, Wang X and Liu Z: Effects of the intestinal microbial metabolite butyrate on the development of colorectal cancer. J Cancer 9: 2510-2517, 2018.
20. Wang YC, Ku WC, Liu CY, Cheng YC, Chien CC, Chang KW and Huang CJ: Supplementation of probiotic butyricicoccus pullicaecorum mediates anticancer effect on bladder urothelial cells by regulating butyrate-responsive molecular signatures. Diagnostics(Basel) 11: 2270, 2021.
21. Kazemi Sefat NA, Mohammadi MM, Hadjati J, Talebi S, Ajami M and Daneshvar H: Sodium butyrate as a histone deacetylase inhibitor affects toll-like receptor 4 expression in colorectal cancer cell lines. Immunol Invest 48: 759-769, 2019.
22. Ji X, Zhou F, Zhang Y, Deng R, Xu W, Bai M, Liu Y, Shao L, Wang X and Zhou L: Butyrate stimulates hepatic gluconeogenesis in mouse primary hepatocytes. Exp Ther Med 17: 1677-1687, 2019.
23. Encarnacao JC, Pires AS, Amaral RA, Gonçalves TJ, Laranjo M, Casalta-Lopes JE, Gonçalves AC, Sarmento-Ribeiro AB, Abrantes AM and Botelho MF: Butyrate, a dietary fiber derivative that improves irinotecan effect in colon cancer cells. J Nutr Biochem 56: 183-192, 2018.
24. Nakano K, Mizuno T, Sowa Y, Orita T, Yoshino T, Okuyama Y, Fujita T, Fujita NO, Matsukawa Y, Tokino T, *et al*: Butyrate activates the WAF1/Cip1 gene promoter through Sp1 sites in a p53-negative human colon cancer cell line. J Biol Chem 272: 22199-22206, 1997.
25. Russo I, Luciani A, De Cicco P, Troncone E and Ciacci C: Butyrate attenuates lipopolysaccharide-induced inflammation in intestinal cells and crohn's mucosa through modulation of antioxidant defense machinery. PLoS One 7: e32841, 2012.
26. Eeckhaut V, Machiels K, Perrier C, Romero C, Maes S, Flahou B, Steppe M, Haesebrouck F, Sas B, Ducatelle R, *et al*: Butyricicoccus pullicaecorum in inflammatory bowel disease. Gut 62: 1745-1752, 2013.
27. Marteau P: Butyrate-producing bacteria as pharmabiotics for inflammatory bowel disease. Gut 62: 1673, 2013.
28. Eeckhaut V, Ducatelle R, Sas B, Vermeire S and Van Immerseel F: Progress towards butyrate-producing pharmabiotics: Butyricicoccus pullicaecorum capsule and efficacy in TNBS models in comparison with therapeutics. Gut 63: 367, 2014.
29. Kilkenny C, Browne W, Cuthill IC, Emerson M and Altman DG; NC3Rs Reporting Guidelines Working Group: Animal research: Reporting in vivo experiments: The ARRIVE guidelines. J Gene Med 12: 561-563, 2010.
30. Soucek K, Gajduskova P, Brazdova M, Hýzd'alová M, Kocí L, Vydra D, Trojanec R, Pernicová Z, Lentvorská L, Hajdúch M, *et al*: Fetal colon cell line FHC exhibits tumorigenic phenotype, complex karyotype, and TP53 gene mutation. Cancer Genet Cytogenet 197: 107-116, 2010.
31. Hayashi Y, Tsujii M, Kodama T, Akasaka T, Kondo J, Hikita H, Inoue T, Tsujii Y, Maekawa A, Yoshii S, *et al*: p53 functional deficiency in human colon cancer cells promotes fibroblast-mediated angiogenesis and tumor growth. Carcinogenesis 37: 972-984, 2016.
32. Rochette PJ, Bastien N, Lavoie J, Guerin SL and Drouin R: SW480, a p53 double-mutant cell line retains proficiency for some p53 functions. J Mol Biol 352: 44-57, 2005.
33. Huang CJ, Yang SH, Huang SM, Lin CM, Chien CC, Chen YC, Lee CL, Wu HH and Chang CC: A predicted protein, KIAA0247, is a cell cycle modulator in colorectal cancer cells under 5-FU treatment. J Transl Med 9: 82, 2011.
34. Ishimine M, Lee HC, Nakaoka H, Orita H, Kobayashi T, Mizuguchi K, Endo M, Inoue I, Sato K and Yokomizo T: The Relationship between TP53 Gene status and carboxylesterase 2 expression in human colorectal cancer. Dis Markers 2018: 5280736, 2018.
35. Abu El Maaty MA, Strassburger W, Qaiser T, Dabiri Y and Wölfl S: Differences in p53 status significantly influence the cellular response and cell survival to 1,25-dihydroxyvitamin D3-metformin cotreatment in colorectal cancer cells. Mol Carcinog 56: 2486-2498, 2017.
36. Li DD, Sun T, Wu XQ, Chen SP, Deng R, Jiang S, Feng GK, Pan JX, Zhang XC, Zeng YX and Zhu XF: The inhibition of autophagy sensitises colon cancer cells with wild-type p53 but not mutant p53 to topotecan treatment. PLoS One 7: e45058, 2012.
37. Bhat UG and Gartel AL: Differential sensitivity of human colon cancer cell lines to the nucleoside analogs ARC and DRB. Int J Cancer 122: 1426-1429, 2008.
38. Kralj M, Husnjak K, Körbler T and Pavelić J: Endogenous p21WAF1/CIP1 status predicts the response of human tumor cells to wild-type p53 and p21WAF1/CIP1 overexpression. Cancer Gene Ther 10: 457-467, 2003.
39. Huang CJ, Lee CL, Yang SH, Chien CC, Huang CC, Yang RN and Chang CC: Upregulation of the growth arrest-specific-2 in recurrent colorectal cancers, and its susceptibility to chemotherapy in a model cell system. Biochim Biophys Acta 1862: 1345-1353, 2016.
40. Leoni BD, Natoli M, Nardella M, Bucci B, Zucco F, D'Agnano L and Felsani A: Differentiation of Caco-2 cells requires both transcriptional and post-translational down-regulation of Myc. Differentiation 83: 116-127, 2012.
41. Livak KJ and Schmittgen TD: Analysis of relative gene expression data using real-time quantitative PCR and the 2(-Delta Delta C(T)) method. Methods 25: 402-408, 2001.
42. Jonkman JE, Cathcart JA, Xu F, Bartolini ME, Amon JE, Stevens KM and Colarusso P: An introduction to the wound healing assay using live-cell microscopy. Cell Adh Migr 8: 440-451, 2014.
43. Ye S, Zhou HB, Chen Y, Li KQ, Jiang SS and Hao K: Crizotinib changes the metabolic pattern and inhibits ATP production in A549 non-small cell lung cancer cells. Oncol Lett 21: 61, 2021.
44. Winkler J, Roessler S, Sticht C, DiGuilio AL, Drucker E, Holzer K, Eiteneuer E, Herpel E, Breuhahn K, Gretz N, *et al*: Cellular apoptosis susceptibility (CAS) is linked to integrin beta1 and required for tumor cell migration and invasion in hepatocellular carcinoma (HCC). Oncotarget 7: 22883-22892, 2016.
45. Zhu JH, Hong DF, Song YM, Sun LF, Wang ZF and Wang JW: Suppression of cellular apoptosis susceptibility (CSE1L) inhibits proliferation and induces apoptosis in colorectal cancer cells. Asian Pac J Cancer Prev 14: 1017-1021, 2013.
46. Nagashima S, Maruyama J, Honda K, Kondoh Y, Osada H, Nawa M, Nakahama KI, Yuasa MI, Kagechika H, Sugimura H, *et al*: CSE1L promotes nuclear accumulation of transcriptional coactivator TAZ and enhances invasiveness of human cancer cells. J Biol Chem 297: 100803, 2021.
47. Snijders AM and Mao JH: Multi-omics approach to infer cancer therapeutic targets on chromosome 20q across tumor types. Adv Mod Oncol Res 2: 215-223, 2016.
48. Behrens P, Brinkmann U and Wellmann A: CSE1L/CAS: Its role in proliferation and apoptosis. Apoptosis 8: 39-44, 2003.
49. Li H, Zhang J, Tong JHM, Chan AWH, Yu J, Kang W and To KF: Targeting the oncogenic p53 mutants in colorectal cancer and other solid tumors. Int J Mol Sci 20: 5999, 2019.
50. Iacopetta B: TP53 mutation in colorectal cancer. Hum Mutat 21: 271-276, 2003.
51. Wang X, Ren Y, Ma S and Wang S: Circular RNA 0060745, a novel circRNA, promotes colorectal cancer cell proliferation and metastasis through miR-4736 sponging. Onco Targets Ther 13: 1941-1951, 2020.

52. Ma S, Yang D, Liu Y, Wang Y, Lin T, Li Y, Yang S, Zhang W and Zhang R: LncRNA BANCR promotes tumorigenesis and enhances adriamycin resistance in colorectal cancer. Aging (Albany NY) 10: 2062-2078, 2018.
53. Cheng DD, Lin HC, Li SJ, Yao M, Yang QC and Fan CY: CSE1L interaction with MSH6 promotes osteosarcoma progression and predicts poor patient survival. Sci Rep 7: 46238, 2017.
54. Ye M, Han R, Shi J, Wang X, Zhao AZ, Li F and Chen H: Cellular apoptosis susceptibility protein (CAS) suppresses the proliferation of breast cancer cells by upregulated cyp24a1. Med Oncol 37: 43, 2020.
55. Li KK, Yang L, Pang JC, Chan AKY, Zhou L, Mao Y, Wang Y, Lau KM, Poon WS, Shi Z and Ng HK: MIR-137 suppresses growth and invasion, is downregulated in oligodendroglial tumors and targets CSE1L. Brain Pathol 23: 426-439, 2013.
56. Beaumont M, Paes C, Mussard E, Knudsen C, Cauquil L, Aymard P, Barilly C, Gabinaud B, Zemb O, Fourre S, *et al*: Gut microbiota derived metabolites contribute to intestinal barrier maturation at the suckling-to-weaning transition. Gut Microbes 11: 1-19, 2020.
57. Silva JPB, Navegantes-Lima KC, Oliveira ALB, Rodrigues DVS, Gaspar SLF, Monteiro VVS, Moura DP and Monteiro MC: Protective mechanisms of butyrate on inflammatory bowel disease. Curr Pharm Des 24: 4154-4166, 2018.
58. Zhao Y, Shi L, Hu C and Sang S: Wheat bran for colon cancer prevention: The synergy between phytochemical alkylresorcinol C21 and intestinal microbial metabolite butyrate. J Agric Food Chem 67: 12761-12769, 2019.
59. Pant K, Mishra AK, Pradhan SM, Nayak B, Das P, Shalimar D, Saraya A and Venugopal SK: Butyrate inhibits HBV replication and HBV-induced hepatoma cell proliferation via modulating SIRT-1/Ac-p53 regulatory axis. Mol Carcinog 58: 524-532, 2019.

This work is licensed under a Creative Commons Attribution-NonCommercial-NoDerivatives 4.0 International (CC BY-NC-ND 4.0) License.

Downloaded on 2023/7/19 04:07:11

2022 Journal Performance Data for: INTERNATIONAL JOURNAL OF ONCOLOGY

ISSN
1019-6439

EISSN
1791-2423

JCR ABBREVIATION
INT J ONCOL

ISO ABBREVIATION
Int. J. Oncol.

Journal Information

EDITION
Science Citation Index Expanded (SCIE)

CATEGORY
ONCOLOGY - SCIE

LANGUAGES
English

REGION
GREECE

1ST ELECTRONIC JCR YEAR
1997

Publisher Information

PUBLISHER
SPANDIDOS PUBL LTD

ADDRESS
POB 18179, ATHENS 116 10, GREECE

PUBLICATION FREQUENCY
12 issues/year

 © 2023 Clarivate

Journal's Performance

Journal Impact Factor

The Journal Impact Factor (JIF) is a journal-level metric calculated from data indexed in the Web of Science Core Collection. It should be used with careful attention to the many factors that influence citation rates, such as the volume of publication and citations characteristics of the subject area and type of journal. The Journal Impact Factor can complement expert opinion and informed peer review. In the case of academic evaluation for tenure, it is inappropriate to use a journal-level metric as a proxy measure for individual researchers, institutions, or articles. Learn more

2022 JOURNAL IMPACT FACTOR	2022 JOURNAL IMPACT FACTOR WITHOUT SELF CITATIONS
5.2	5.2

Journal Impact Factor Trend 2022

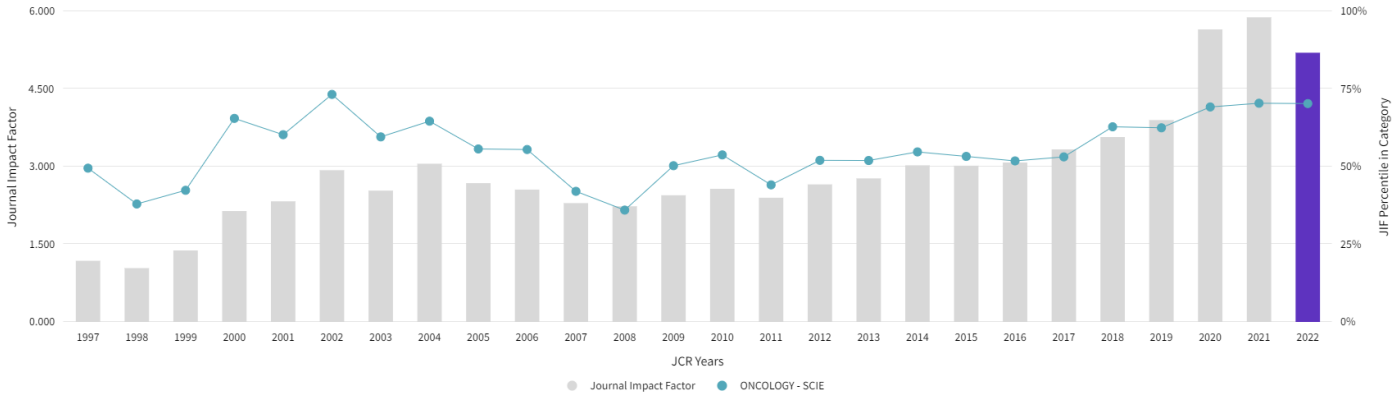

 © 2023 Clarivate

Journal Impact Factor is calculated using the following metrics

Citations in 2022 to items published in 2020 (**1,259**) - 2021 (**586**)	=	**1,845**	=	**5.2**
Number of citable items in 2020 (**229**) + 2021 (**124**)		**353**		

Journal Impact Factor without self cites is calculated using the following metrics

Citations in 2022 to items published in 2020 (**1,259**) + 2021 (**586**) - Self Citations in 2022 to items published in 2020 (**7**) + 2021 (**7**)	=	**1,845 - 14**	=	**5.2**
Number of citable items in 2020 (**229**) + 2021 (**124**)		**353**		

 © 2023 Clarivate

Journal Impact Factor Contributing Items

Citable Items (353)

TITLE	CITATION COUNT
Anticancer peptide: Physicochemical property, functional aspect and trend in clinical application (Review) Authors: Chiangjong, Wararat;Chutipongtanate, Somchai;Hongeng, Suradej Volume: 57 Accession number: WOS:000563562900005 Document Type: Review	58
Triple-negative breast cancer therapy: Current and future perspectives (Review) Authors: Won, Kwang-Ai;Spruck, Charles Volume: 57 Accession number: WOS:000593969700001 Document Type: Review	58
A multidisciplinary approach remains the best strategy to improve and strengthen the management of ovarian cancer (Review) Authors: Falzone, Luca;Scandurra, Giuseppa;Lombardo, Valentina;Gattuso, Giuseppe;Lavoro, Alessandro;Distefano, Andrea Benedetto;Scibilia, Giuseppe;Scollo, Paolo Volume: 59 Accession number: WOS:000662993000001 Document Type: Review	30
Current molecular and clinical insights into uveal melanoma (Review) Authors: Fallico, Matteo;Avitabile, Teresio;Raciti, Giuseppina;Longo, Antonio;Reibaldi, Michele;Bonfiglio, Vincenza;Russo, Andrea;Caltabiano, Rosario;Gattuso, Giuseppe;Falzone, Luca Volume: 58 Accession number: WOS:000623255400001 Document Type: Review	26
Mechanisms and management of 3rd-generation EGFR-TKI resistance in advanced non-small cell lung cancer (Review) Authors: He, Jingyi;Huang, Zhengrong;Han, Linzhi;Gong, Yan;Xie, Conghua Volume: 59 Accession number: WOS:000714644100001 Document Type: Review	25

Showing 1-5 rows of 353 total (use export in the relevant section to download the full table)

 © 2023 Clarivate

Journal Impact Factor Contributing Items

Citing Sources (613)

SOURCE NAME	COUNT
FRONTIERS IN ONCOLOGY	97
CANCERS	89
INTERNATIONAL JOURNAL OF MOLECULAR SCIENCES	87
FRONTIERS IN IMMUNOLOGY	46
FRONTIERS IN GENETICS	39
FRONTIERS IN PHARMACOLOGY	36
CELLS	32
BIOENGINEERED	23
JOURNAL OF ONCOLOGY	22
SCIENTIFIC REPORTS	22
BIOMEDICINES	21
MOLECULES	19
BIOMEDICINE & PHARMACOTHERAPY	17
FRONTIERS IN CELL AND DEVELOPMENTAL BIOLOGY	17
CANCER CELL INTERNATIONAL	14
INTERNATIONAL JOURNAL OF ONCOLOGY	14
MOLECULAR BIOLOGY REPORTS	14
CELL DEATH & DISEASE	13
ONCOLOGY LETTERS	12
BIOMOLECULES	11

Showing 1-20 rows of 613 total (use export in the relevant section to download the full table)

 © 2023 Clarivate

Journal Citation Indicator (JCI)

0.98

The Journal Citation Indicator (JCI) is the average Category Normalized Citation Impact (CNCI) of citable items (articles & reviews) published by a journal over a recent three year period. The average JCI in a category is 1. Journals with a JCI of 1.5 have 50% more citation impact than the average in that category. It may be used alongside other metrics to help you evaluate journals. Learn more

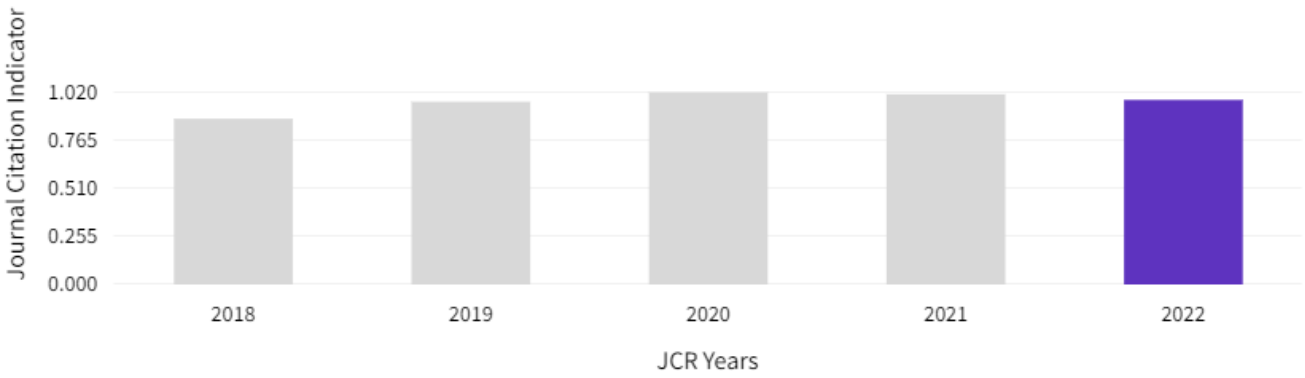

Total Citations

20,086

The total number of times that a journal has been cited by all journals included in the database in the JCR year. Citations to journals listed in JCR are compiled annually from the JCR years combined database, regardless of which JCR edition lists the journal.

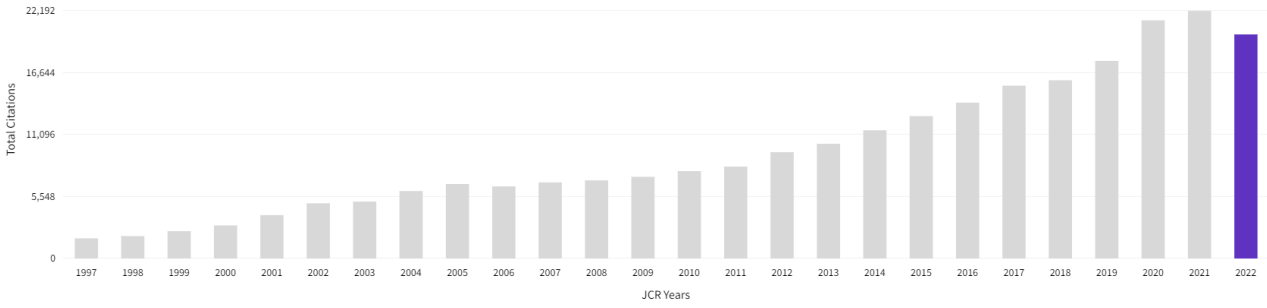

 © 2023 Clarivate

Citation Distribution

The Citation Distribution shows the frequency with which items published in the year or two years prior were cited in the JCR data year (i.e., the component of the calculation of the JIF). The graph has similar functionality as the JIF Trend graph, including hover-over data descriptions for each data point, and an interactive legend where each data element's legend can be used as a toggle. You can view Articles, Reviews, or Non-Citable (other) items to the JIF numerator. Learn more

ARTICLE CITATION MEDIAN	REVIEW CITATION MEDIAN	UNLINKED CITATIONS
4	5	9

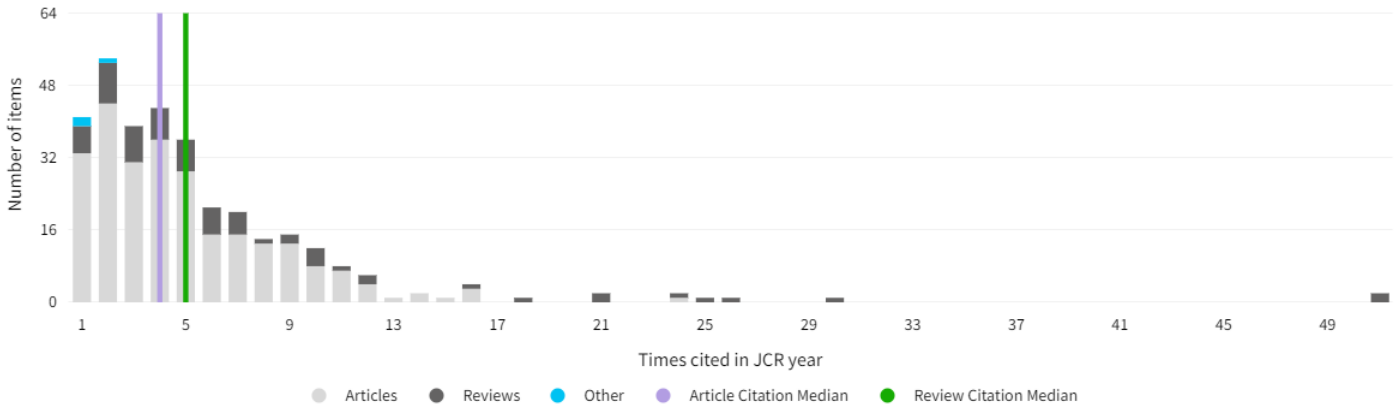

0 times cited

ARTICLES	REVIEWS	OTHER
23	6	30

 © 2023 Clarivate

Open Access (OA)

The data included in this tile summarizes the items published in the journal in the JCR data year and in the previous two years. This three-year set of published items is used to provide descriptive analysis of the content and community of the journal.Learn more

Items

TOTAL CITABLE
488

% OF CITABLE OA
65.78%

CITABLE

GOLD OPEN ACCESS
321 / 59.12%

SUBSCRIPTION OR BRONZE
167 / 30.76%

NON-CITABLE

OTHER (NON-CITABLE ITEMS)
55 / 10.13%

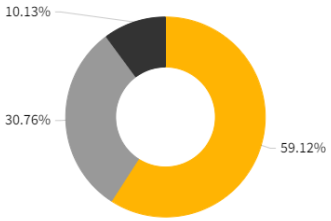

Citations*

TOTAL CITABLE
2,032

% OF CITABLE OA
72.24%

CITABLE

GOLD OPEN ACCESS
1,468 / 71.51%

SUBSCRIPTION OR BRONZE
564 / 27.47%

NON-CITABLE

OTHER (NON-CITABLE ITEMS)
5 / 0.24%

UNLINKED CITATIONS
16 / 0.78%

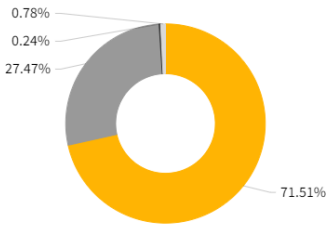

* Citations in 2022 to items published in (2020-2022)

 © 2023 Clarivate

Rank by Journal Impact factor

Journals within a category are sorted in descending order by Journal Impact Factor (JIF) resulting in the Category Ranking below. A separate rank is shown for each category in which the journal is listed in JCR. Data for the most recent year is presented at the top of the list, with other years shown in reverse chronological order. Learn more

EDITION

Science Citation Index Expanded (SCIE)

CATEGORY

ONCOLOGY

72/241

JCR YEAR	JIF RANK	QUARTILE	JIF PERCENTILE
2022	72/241	Q2	70.3
2021	73/245	Q2	70.41
2020	75/242	Q2	69.21
2019	92/244	Q2	62.50
2018	86/230	Q2	62.83
2017	105/223	Q2	53.14
2016	105/217	Q2	51.84
2015	100/213	Q2	53.29
2014	96/211	Q2	54.74
2013	98/203	Q2	51.97
2012	95/197	Q2	52.03
2011	110/196	Q3	44.13
2010	86/185	Q2	53.78
2009	83/166	Q2	50.30
2008	92/143	Q3	36.01
2007	77/132	Q3	42.05
2006	57/127	Q2	55.51
2005	55/123	Q2	55.69
2004	44/123	Q2	64.63
2003	49/120	Q2	59.58
2002	31/114	Q2	73.25
2001	43/107	Q2	60.28
2000	36/103	Q2	65.53
1999	61/105	Q3	42.38
1998	65/104	Q3	37.98
1997	52/102	Q3	49.51

© 2023 Clarivate

Rank by Journal Citation Indicator (JCI)

Journals within a category are sorted in descending order by Journal Citation Indicator (JCI) resulting in the Category Ranking below. A separate rank is shown for each category in which the journal is listed in JCR. Data for the most recent year is presented at the top of the list, with other years shown in reverse chronological order.Learn more

CATEGORY

ONCOLOGY

79/317

JCR YEAR	JCI RANK	QUARTILE	JCI PERCENTILE
2022	79/317	Q1	75.24
2021	80/318	Q2	75.00
2020	83/310	Q2	73.39
2019	90/308	Q2	70.94
2018	106/302	Q2	65.07
2017	105/290	Q2	63.97

 © 2023 Clarivate

Citation network

Cited Half-life

7.3 years

The Cited Half-Life is the median age of the items in this journal that were cited in the JCR year. Half of a journal's cited items were published more recently than the cited half-life.

TOTAL NUMBER OF CITES	NON-SELF CITATIONS	SELF CITATIONS
20,086	19,985	101

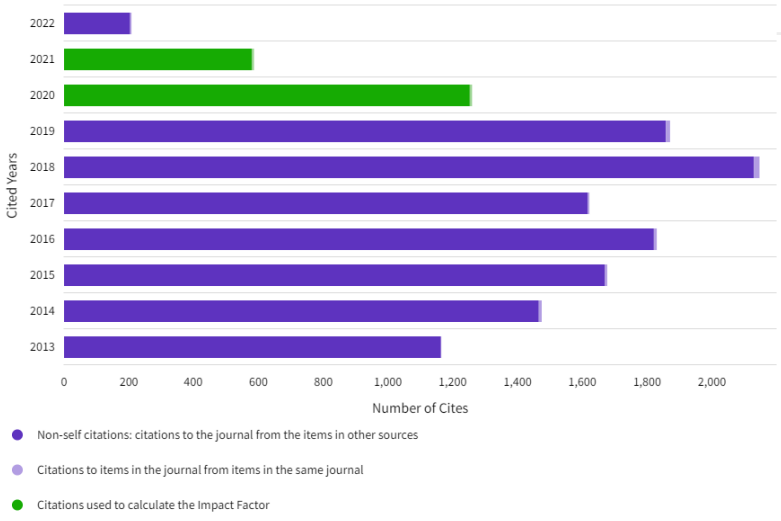

# OF CITES FROM 2022	CUMULATIVE %	# OF CITING SOURCES
20,086 citations	**100.00%**	**2,376 sources**
208 citations	1.04%	106 sources
586 citations	3.95%	281 sources
1,259 citations	10.22%	489 sources
1,870 citations	19.53%	679 sources
2,146 citations	30.22%	684 sources
1,621 citations	38.29%	618 sources
1,829 citations	47.39%	658 sources
1,676 citations	55.74%	673 sources
1,474 citations	63.07%	585 sources
1,164 citations	68.87%	520 sources
Previous years: 6,253 citations		

 © 2023 Clarivate